

Effect of Geometric Azimuthal Asymmetries of PPM Stack on Electron Beam Characteristics

Carol L. Kory, *Senior Member*

Abstract - A three-dimensional (3D) beam optics model has been developed using the electromagnetic particle-in-cell (PIC) code MAFIA. The model includes an electron beam with initial transverse velocity distribution focused by a periodic permanent magnet (PPM) stack. All components of the model are simulated in three dimensions allowing several azimuthally asymmetric traveling wave tube (TWT) characteristics to be investigated for the first time. These include C-magnets, shunts and magnet misalignment and their effects on electron beam behavior. The development of the model is presented and 3D TWT electron beam characteristics are compared in the absence of and under the influence of the azimuthally asymmetric characteristics described.

I. INTRODUCTION

TWT developers have found experimentally that spent beam data entering the collector are often azimuthally asymmetric and/or shifted from the tube's central axis making efficient collection very difficult [i]. Overall TWT efficiency is significantly impacted since it is highly dependent on collector efficiency. A shifting of the electron beam off the tube's central axis can also lead to increased beam/circuit interception, also reducing TWT efficiency and causing excessive heating of the RF circuit. In order to prevent or compensate for this adverse beam behavior, it is essential to identify its source and quantify its effects. The 3D electron optics model was used to investigate several geometric azimuthally asymmetric characteristics of the focusing structure suspected to cause this asymmetric beam behavior, including C-magnets, shunts and magnet misalignment. For the first time, the significance of these geometrically asymmetric characteristics was computationally demonstrated in terms of percent ripple, percent transmission, maximum and minimum beam radii, beam profiles and beam shift off the central axis.

Typically, electron optics codes are used for designing beam focusing structures and are based on balancing diverging forces due to space charge fields, beam rotation, and transverse velocity components due to thermal effects at the cathode and scattering from the electron gun grid. In general, these codes track the beam from the gun downstream by solving equations of motion for the electron beam in static electric and magnetic fields. RF fields generated by the slow-wave circuit are neglected. The 3D electron optics model presented here was developed using MAFIA (Solution of **MA**xwell's equations by the **F**inite-**I**ntegration-**A**lgorithm) [ii, iii], a powerful

electrodynamic code incorporating several modules. The modules used in this study are M (mesh generator), S (static solver), TS3 (3D particle-in-cell (PIC) solver) and P (postprocessor).

The TWT used as a model is a 40 Watt, 18-40 GHz helical TWT designated the 8916H, developed by Hughes for the millimeter-wave power module (MMPM) [iv]. The operating parameters for the tube are shown in Table I. The cross-sectional and top views of a section of the baseline periodic permanent magnet (PPM) stack used for focusing are shown in Figure 1. The focusing stack consists of a sequence of iron pole pieces and opposite polarity samarium cobalt $\text{Sm}_2\text{Co}_{17}$ magnets with magnetic period L .

II. SIMULATION AND ANALYSIS

The mesh generator of MAFIA was used to model the actual dimensions of the Hughes 8916H TWT PPM stack [iv]. The static solver was used to define the actual material properties, including the provided experimental B-H curve [v] for the iron pole pieces and a fixed magnetization and permeability for the magnets. The static solver was then used to calculate the static fields in the structure and the on-axis longitudinal component of the magnetic flux density B_z was compared to experiment with excellent agreement [vi]. The fields were loaded into the PIC solver, which was used to simulate an electron beam immersed in the previously calculated static fields from the PPM stack. The modeled volume is reduced for the PIC simulations by including only a portion of the PPM stack geometry (See Figure 2).

The PIC solver computes the time-integration of electromagnetic fields simultaneously with the time integration of the equations of motion of charged particles that move under the influence of those fields. Fields caused by those moving charges are also taken into account; thus, effects like space charge and magnetic forces between particles are fully simulated [vii]. Particle motion is unrestricted, so particle trajectories can cross paths and move in three dimensions under the influence of 3D electric and magnetic fields. Correspondingly, there is no limit on the current density distribution of the electron beam.

Simulations were completed for beams with and without initial transverse velocities. In actual beams, initial transverse velocities are present due to gun characteristics such as finite beam temperature, electron gun imperfections and scattering from grid wires. The simulated electron beam was initialized with a transverse velocity

distribution as one might find at the beam waist using a diode electron gun due to beam compression and the finite temperature of the cathode. The initial transverse velocity distribution was based on a Gaussian probability distribution with standard deviation

$$\sigma = \sqrt{\frac{kT_c C_r}{m}} \quad (1)$$

where k is Boltzman's constant, T_c is cathode temperature in Kelvin, m is electron mass and C_r is the beam compression defined by

$$C_r = \left(\frac{r_c}{r_{95}} \right)^2. \quad (2)$$

The beam radius containing 95% of the beam current is designated r_{95} and r_c is the cathode disk radius.

The baseline model incorporates about six magnetic periods of the 8916H TWT PPM stack with beam parameters as listed in Table I. A focusing strength commensurate with twice the Brillouin field B_B was used, or an rms value of [viii]

$$2B_B = 2 \left[0.83e - 3 \frac{I_o^{1/2}}{bV_o^{1/4}} \right] T \quad (1)$$

for a beam with initial radius b , current I_o and voltage V_o .

In this report, the baseline model of several azimuthally symmetric magnetic periods is compared to the model including the geometric azimuthally asymmetric PPM stack characteristics in terms of percent ripple, percent transmission, two-dimensional (2D) beam profiles, maximum and minimum radii including 95 percent of the beam current and beam shift off the tube's central axis. The percent ripple is calculated as

$$\% \text{ ripple} = \frac{\Delta}{d_{avg}} 100 \quad (3)$$

where Δ is the difference between the maximum and minimum radius containing 95% of the beam current and d_{avg} is the average beam diameter containing 95 percent of the beam current. The beam was simulated long enough in time for all particles to be dissipated in the beam tunnel or the collector plate placed at the longitudinal end of the tunnel (See Figure 2). The percent transmission was calculated as the percentage of beam energy dissipated in the collector plate. Figure 2 shows the 2D beam profiles for the baseline simulations with and without initial transverse velocities.

III. C-MAGNETS

C-magnets are used at the input and output of the TWT to allow for the inclusion of waveguides to couple the RF signal into and out of the tube. The input and output C-magnets and their orientations in the Cartesian coordinate system are shown in Figure 3 and Figure 4, respectively. The input and output C-magnets differ because coaxial and waveguide couplers are used at the input and output, respectively. The magnetizations of the C-magnets were adjusted in the model so that the field strengths on-axis were equal to twice the Brillouin field.

A. Discussion of the effects of C-magnet asymmetries

Before presenting the results of the C-magnet simulations, it is helpful to discuss the effects of the azimuthal asymmetry of the C-magnets on the field configuration and the corresponding electron beam behavior. Recall that when the beam enters the PPM stack, it is initially exposed to radially directed magnetic flux lines at the first pole piece. The force F_B on an electron with charge e and velocity u due to the magnetic flux density B is expressed as

$$F_B = -e(u \times B). \quad (2)$$

Overall, the beam starts to rotate. As the beam travels down the tunnel it experiences a strong longitudinally directed magnetic flux density due to the first magnet. This flux interacts with the rotating beam to produce an azimuthally symmetric radially directed force toward the central axis. Thus, the beam is focused and because of the azimuthal symmetry, it retains its central position on the transverse plane.

In the configurations shown in Figure 3 and Figure 4, the C-magnets introduce asymmetries in the y direction since the cutout portion of the magnet is in the positive- y half of the transverse plane. A zoomed in arrow plot of the magnetic flux density in the vicinity of the output C-magnet is shown in Figure 5 where the strength of the field is proportional to the size of the arrows. The percent difference between the fields in positive- and negative- y directions of the transverse plane at $x=0$ for the z and y components of the fields are plotted in Figure 6 and Figure 7, respectively, for both the input and output C-magnets. The B-fields over the input C-magnet are oriented in the same directions as those shown in Figure 5. Figure 6 corresponds to a longitudinal position commensurate with the center of the C-magnet and Figure 7 corresponds to the center of the pole piece following the C-magnet (the center of the pole piece preceding the C-magnet has a similar configuration). As expected, the fields are stronger over the negative- y half of the transverse plane. The input C-magnet case shows a very slight difference between the fields over the positive and negative halves of the transverse plane; however, the output C-magnet shows a larger variation, especially in B_y .

Consider again the force equation of (2) applied to the case where the beam is exposed to asymmetric fields that are stronger in the negative- y half of the transverse plane (as would be introduced by the C-magnets with the chosen orientation in the Cartesian coordinate system). By summing forces on the electron beam, it was shown in [vi] that as the beam propagates down the beam tunnel, it will be shifted in the positive- y direction and alternately in the positive- and negative- x directions depending on the orientation of the field at the pole piece it passed through most recently.

B. Input C-magnet

Simulations were completed including the input C-magnet (shown in Figure 3) placed as the second magnet in the PPM stack. The corresponding 2D beam profiles for the beam neglecting and including initial transverse velocities are shown in Figure 8. The beam cross-sections at several longitudinal points were monitored and it was found that there was no significant beam shift off the tube's central axis with the input C-magnet included.

Table II lists the maximum and minimum radii containing 95 percent of the beam current (r_{\max} and r_{\min} , respectively) normalized to the initial beam radius b , percent ripple and percent transmission for the simulations with and without the input C-magnet, and with and without initial transverse velocities. There is a significant reduction in the percent ripple for the beam without transverse velocities including the input C-magnet. Comparing Figure 8 and Figure 2 shows that the longitudinal length of the input C-magnet is larger than the length of the nominal magnets in the PPM stack. Consequently, it experiences a reduction in inward focusing force. Thus, the diameter of the beam is increased compared to the case without the input C-magnet, and a corresponding decrease in the percent ripple occurs. When initial transverse velocities are included, this reduction in inward force causes the interception of the beam with the tunnel to increase, thus reducing the percent transmission.

C. Output C-magnet

First, simulations were completed for a beam without initial transverse velocities and with the output C-magnet (shown in Figure 4) placed as the second last magnet in the PPM stack. The 2D beam profile is shown in Figure 9 (a). With respect to the average

beam radius, at a longitudinal position corresponding to point A on Figure 9 the beam is shifted about six percent and eight percent in the positive-y and positive-x directions, respectively. At point B, the beam is shifted about 24 percent and two percent in the positive-y and positive-x directions, respectively. At point C, the beam is shifted about 20 percent and eight percent in the positive-y and negative-x directions, respectively. These results are summarized in Table III. The beam cross-section at a longitudinal point corresponding to point B of Figure 9 is shown in Figure 10 (a) demonstrating the beam shift from the tube's central axis. The grid lines corresponding to the tube's central axis were darkened to illuminate the shift off the axis.

Next, simulations were completed for a beam with initial transverse velocities with the output C-magnet. The 2D beam profile plot is shown in Figure 9 (b). With respect to the average beam radius, at a longitudinal position corresponding to point B on Figure 9, the beam is shifted about 14 percent and zero percent in the positive-y and positive-x directions, respectively. At point C, the beam is shifted about 10 percent and four percent in the positive-y and negative-x directions, respectively. At point A, the beam is intercepting the tunnel making it difficult to determine the beam's shift off the central axis. These results are also summarized in Table III. The beam cross-section at a longitudinal point corresponding to point B of Figure 9 is shown in Figure 10 (b).

The maximum and minimum radii containing 95 percent of the beam current, percent ripple and percent transmission for the simulations with and without the output C-magnet, and with and without initial transverse velocities are listed in Table II. Compared to the baseline model, there is no change in the percent ripple or percent transmission for the beam without transverse velocities including the output C-magnet.

Since the output C-magnet is placed at the end of the beam tunnel, the effect of the increased C-magnet longitudinal length does not have the same effect as the case where the input C-magnet was included. However, we would expect the beam's divergence to increase from the reduced focusing force if it were allowed to propagate for a longer longitudinal length. For the case where initial transverse velocities were included, the case including the output C-magnet shows a slight decrease in the percent transmission. This is expected since the beam is shifted off the central axis and will therefore experience an increase in beam/tunnel interception.

IV. SHUNTS

Shunts are rectangular iron pieces often fixed to the PPM stack pole pieces at the input section of the tube to selectively decrease the focusing strength in order to improve beam transmission. The application of shunts is done manually by a skilled technician, and the procedure is tedious, time-intensive and often based on trial-and-error. The shunts are applied to the top of the tube; thus, azimuthal symmetry of the focusing stack is interrupted. Although they are typically added during RF focusing, they are also typically added at the input section of the tube where the RF forces are minimal.

The dimensions of the shunts are on the order of 0.02 x 0.07 x 0.2 inches. Because several are usually applied to one pole piece, the simulations have been simplified by modeling a solid washer with the same radius and longitudinal length over the entire x, positive-y half of the transverse plane (See Figure 11). The shunt was added to the third pole piece of the stack in an attempt to alleviate the drastic pinch in beam diameter for the baseline beam without initial transverse velocities (See Figure 2 (a)). The changes in the peak values of B_z on the axis over the first several magnets with the addition of the shunt are given in Table IV (the shunt is applied between magnets two and three). The peak field changes by about three percent in the vicinity of the shunt, which is within the tolerance for the magnets. The percent difference in B_y between the positive- and negative-y directions of the transverse plane ($x = 0$, $z =$ the center of the pole piece with the shunt) was found to be less than -0.5 percent. The percent difference in B_z between the positive-and negative-y directions of the transverse plane ($x = 0$, $z =$ the center of the magnet following the shunt) was found to be less than -0.003 percent.

There was only a very slight change in the beam behavior compared to the case without the shunt. The maximum and minimum radii containing 95 percent of the beam current, percent ripple and percent transmission for the simulations including the shunt are listed in Table II. The percent ripple is decreased slightly from 85.7 to 82.9 percent. This decrease is due to a very slight enlargement of the beam diameter at the first minimum diameter located longitudinally at a point just after the shunt. The diameter of the beam with the shunt at a longitudinal position commensurate with the end of the modeled stack was found to decrease slightly compared with the baseline simulations.

For the simulations where the shunt and initial transverse velocities were included, there was a very slight change in the beam behavior compared to the case without the shunt. As listed in Table II, the percent ripple is increased slightly from 14.64 to 16.44 percent with a corresponding slight decrease in percent transmission from 99.11 to 98.84 percent. This increase in percent ripple is due to the slight enlargement of the beam diameter at the first minimum diameter located longitudinally at a point just after the shunt. The diameter of the beam at a longitudinal position commensurate with the end of the modeled stack was increased slightly with the shunt included compared with the baseline simulations.

V. MISALIGNED MAGNETS

Positioning the magnets so that their central axis is accurately aligned with the central axis of the tube is challenging. Thus, it is a strong possibility that one or more magnets will be misaligned relative to the tube's central axis. To investigate the effect this will have on beam characteristics, the third magnet in the PPM stack was arbitrarily chosen and adjusted so that its central axis was located 0.7 percent and 1.0 percent of the magnet outer diameter (OD) in the positive-y direction. Compared to the baseline model, the corresponding longitudinal component of the magnetic flux density on the axis changed very slightly with an average increase of 0.59 percent for the 0.7 percent shift and 0.66 percent for the 1.0 percent shift. For both cases, the percent differences in B_y between the positive- and negative-y directions of the transverse plane ($x = 0$, $z =$ the center of the pole piece following the misaligned magnet) were found to be less than 0.4 percent. The percent differences in B_z between the positive- and negative-y directions of the transverse plane ($x = 0$, $z =$ the center of the misaligned magnet) were found to be less than 0.03 percent. The effects of the misaligned magnets on beam characteristics were found to be negligible.

VI. CONCLUSIONS

The 3D MAFIA electron optics model was used to investigate the effects of geometric azimuthally asymmetric characteristics of the PPM stack on electron beam behavior. In particular, maximum and minimum beam radii containing 95 percent of the beam current, percent ripple, percent transmission, 2D beam profiles and beam position relative to the tube's central axis were compared for a baseline azimuthally symmetric PPM model and models including C-magnets, shunts and misaligned magnets.

When the input magnet was included, a significant decrease in percent ripple (from 85.7 to 58.8 percent) was observed for the beam excluding initial transverse velocities. It was found that while the beam was exposed to the asymmetric fields due to the output C-magnet, it was shifted upward off the central tube axis. Simultaneously, it was alternately shifted to the left and right depending on the orientation of the field at the pole piece it passed through most recently. The most significant shift was at a longitudinal position corresponding to the center of the magnet following the output C-magnet where the beam without initial transverse velocities was shifted off the central axis 20 percent upward and eight percent to one side relative to the average beam radius.

A small effect was found on percent ripple and percent transmission when shunts were added in the beam optics simulations, with negligible beam shift from the central axis. The peak longitudinal component of the magnetic flux density changed by about three percent, which is within the manufacturer's tolerance for the magnets. The effects of the misaligned magnets on beam characteristics were found to be negligible.

As a result of these simulations, it appears that the C-magnets have the largest effect on beam behavior. The resulting beam shift off the central axis due to the output

C-magnet implies the need for an azimuthally asymmetric collector or some mechanism to shift the beam back onto the central axis before azimuthally symmetric collection. Using the 3D beam optics model developed here, the simulated spent beam data with the output C-magnet included, can be used as input into a collector simulation code to design such an azimuthally asymmetric collector or shifting correction mechanism. This could translate into a significant improvement in collector efficiency, and thus overall TWT efficiency. These results also indicate that the effect of these azimuthal characteristics may contribute to disagreement between measured TWT performance and that predicted by conventional 2D codes.

Table I Operating parameters for Hughes 8916H helical TWT

Frequency, f (GHz)	18 – 40
Beam voltage, V_o (kV)	7.6
Beam current, I_o (mA)	81.0
Initial beam radius/helix average radius, b/a	0.5

Table II Beam characteristics for PPM stack simulations.

Simulation configuration	r_{\max}/b	r_{\min}/b	Percent ripple	Percent transmission
<i>Excluding initial transverse velocities</i>				
Baseline	1.200	0.092	85.70	100
Input C-magnet	1.245	0.323	58.77	100
Output C-magnet	1.200	0.092	85.70	100
Shunt	1.187	0.111	82.92	100
<i>Including initial transverse velocities</i>				
Baseline	1.468	1.093	14.64	99.11
Input C-magnet	1.520	1.132	14.63	97.00
Output C-magnet	1.481	1.087	15.34	98.73
Shunt	1.523	1.093	16.44	98.84

Table III Beam shift off central axis at longitudinal points A, B and C (see Figure 9)

due to inclusion of output C-magnet.

Longitudinal position	Shift off central axis (percent of average beam radius)			
	<i>Excluding initial transverse velocities</i>		<i>Including initial transverse velocities</i>	
	x-direction	y-direction	x-direction	y-direction
A	8	6	(Intercepting)	(Intercepting)
B	2	24	0	14
C	-8	20	-4	10

Table IV Difference in peak values of on-axis longitudinal components of magnetic flux density for PPM stack with shunt.

Magnet number	Difference (Percent)
1	3.24
2	-2.67
3	-2.82
4	3.32
5	-2.78
6	1.12
7	-1.27
8	0.31
9	-0.68
10	0.04

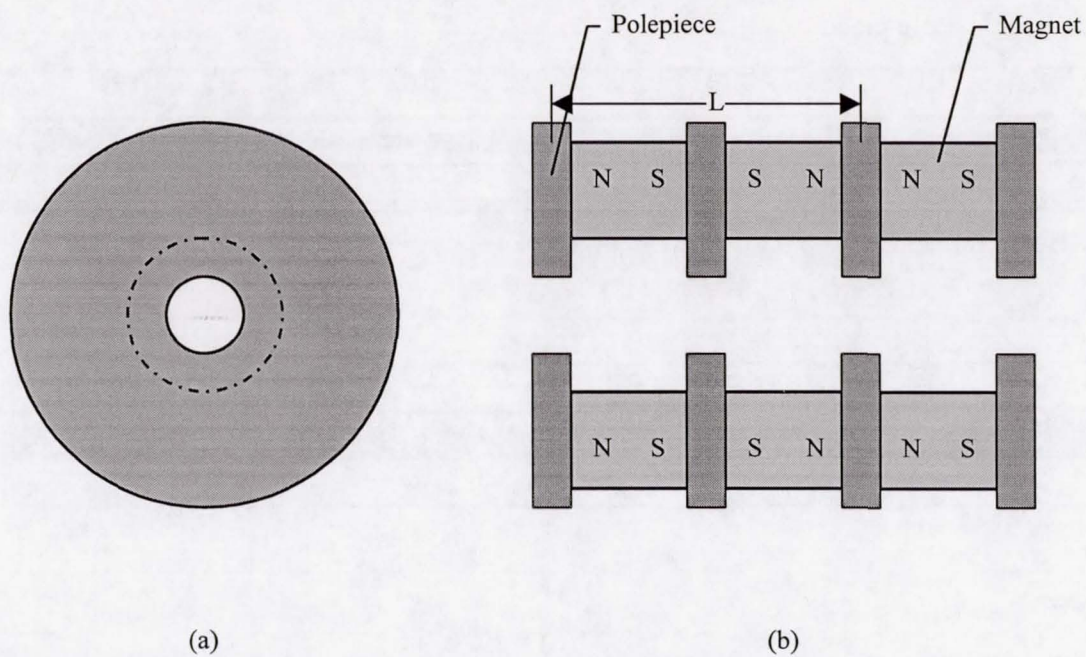


**Figure 1 (a) Cross-sectional and (b) top views of a section of the 8916H TWT
periodic permanent magnet focusing stack**

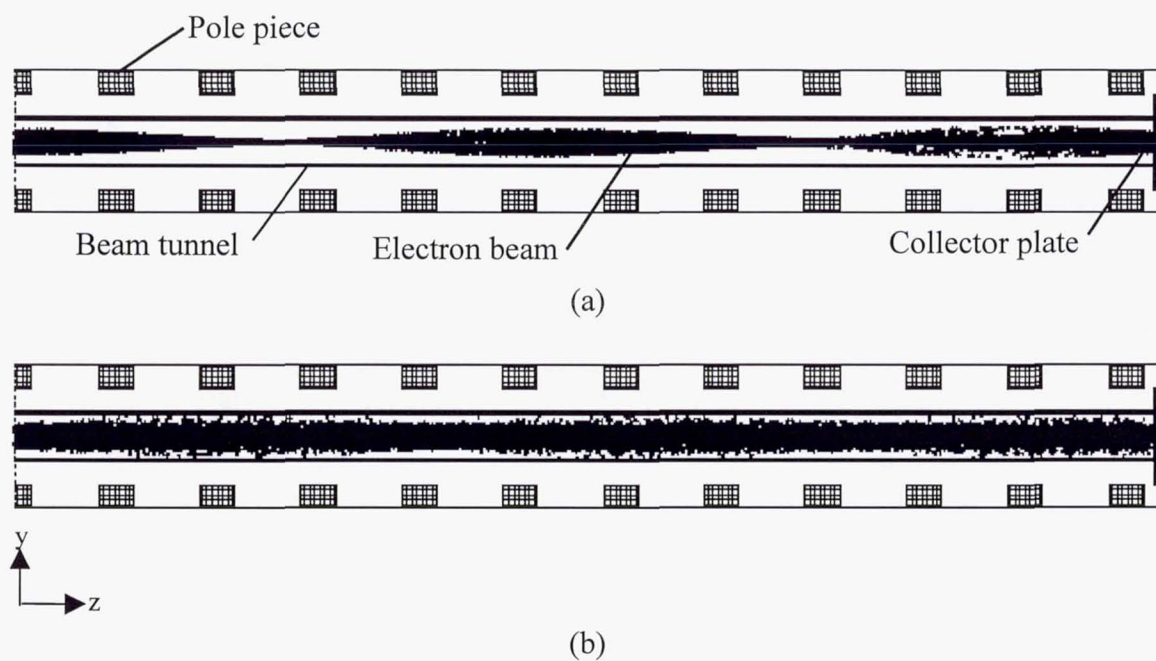


Figure 2 Two-dimensional beam profiles for several magnetic periods of PPM stack baseline model (a) without initial transverse velocities and (b) with initial transverse velocities

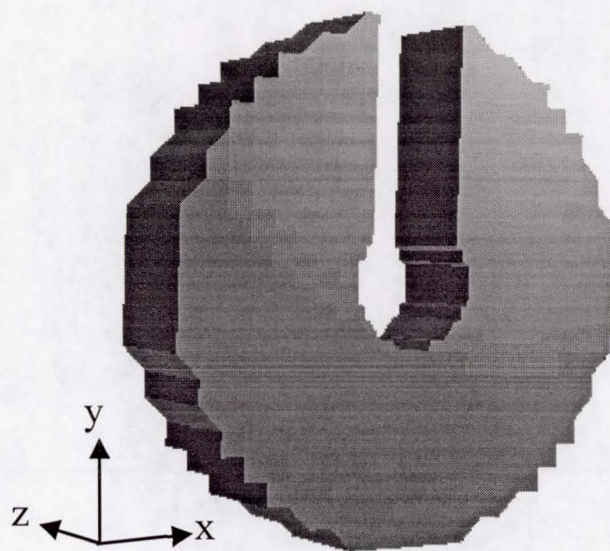


Figure 3 8916H TWT input C-magnet

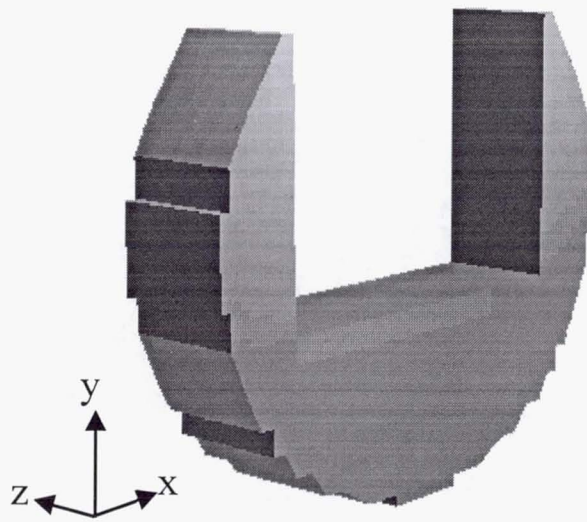


Figure 4 8916H TWT output C-magnet

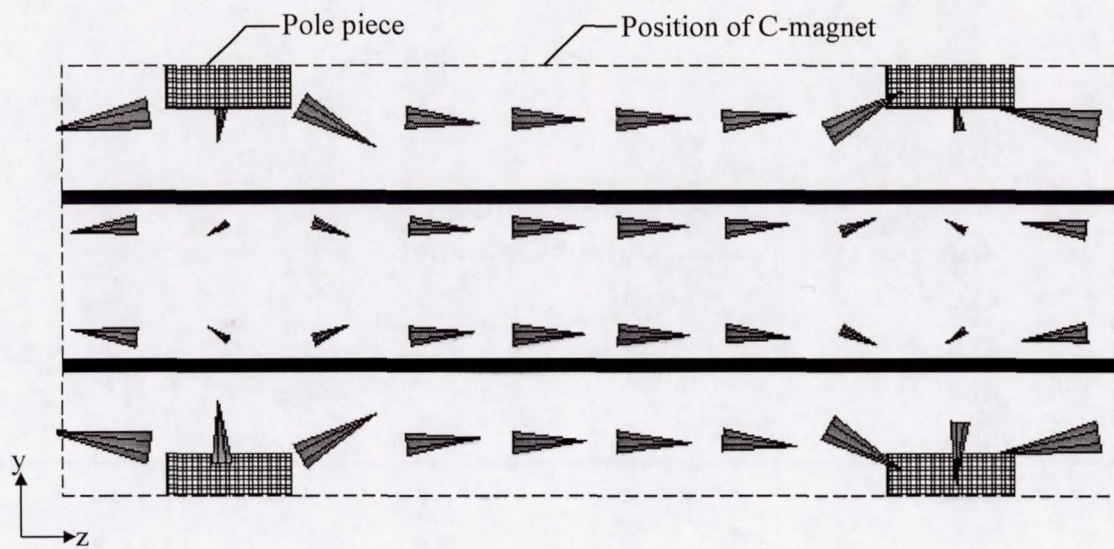


Figure 5 Zoomed in arrow plot of magnetic flux density over the simulation space in the presence of the output C-magnet

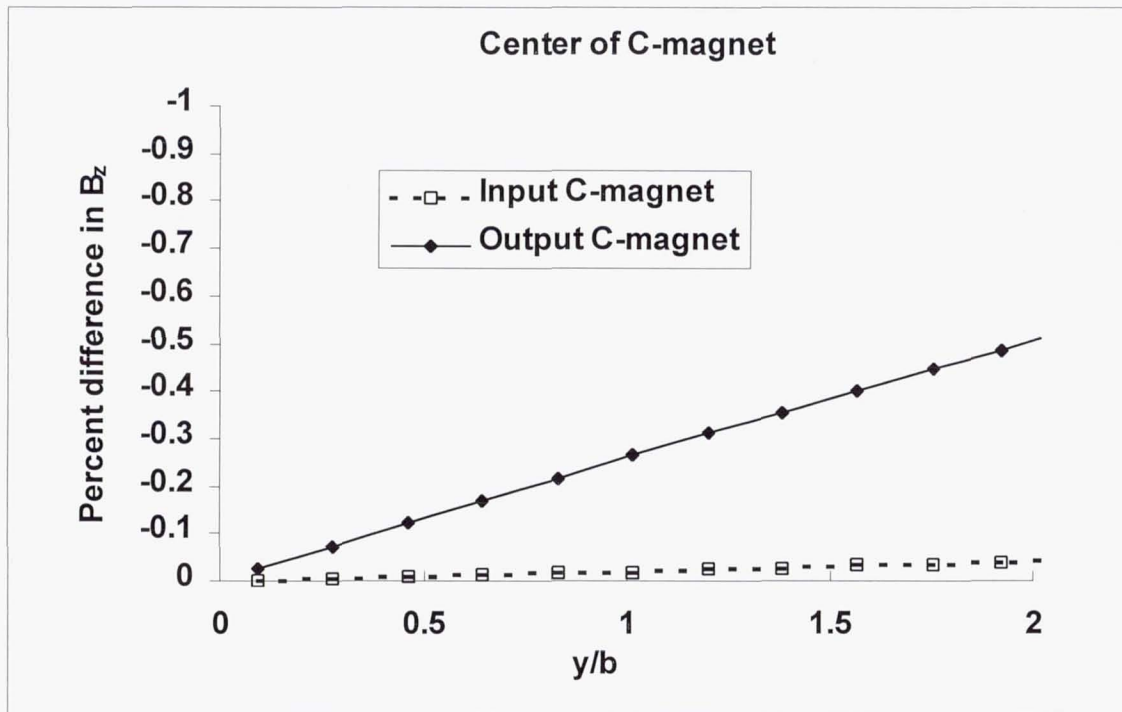


Figure 6 Percent difference in B_z between the positive and negative halves of the transverse plane for input and output C-magnets at $x=0$ and $z =$ the center of the C-magnet

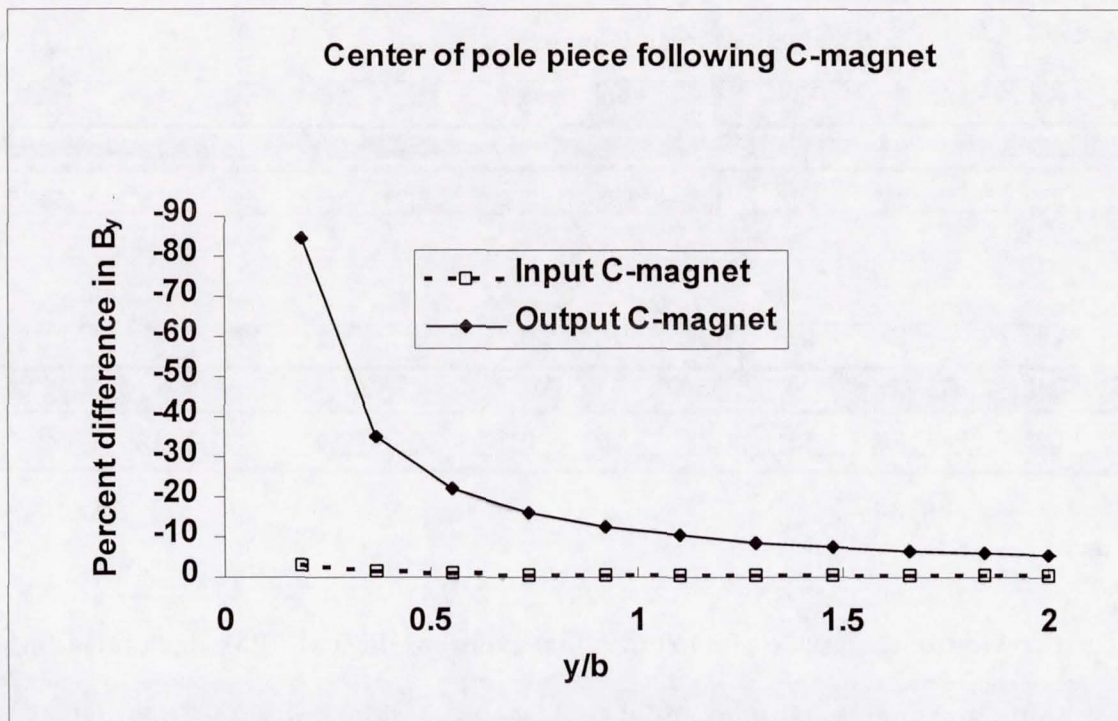


Figure 7 Percent difference in B_y between the positive and negative halves of the transverse plane for input and output C-magnets magnets at $x=0$ and $z =$ the center of the pole piece following the C-magnet

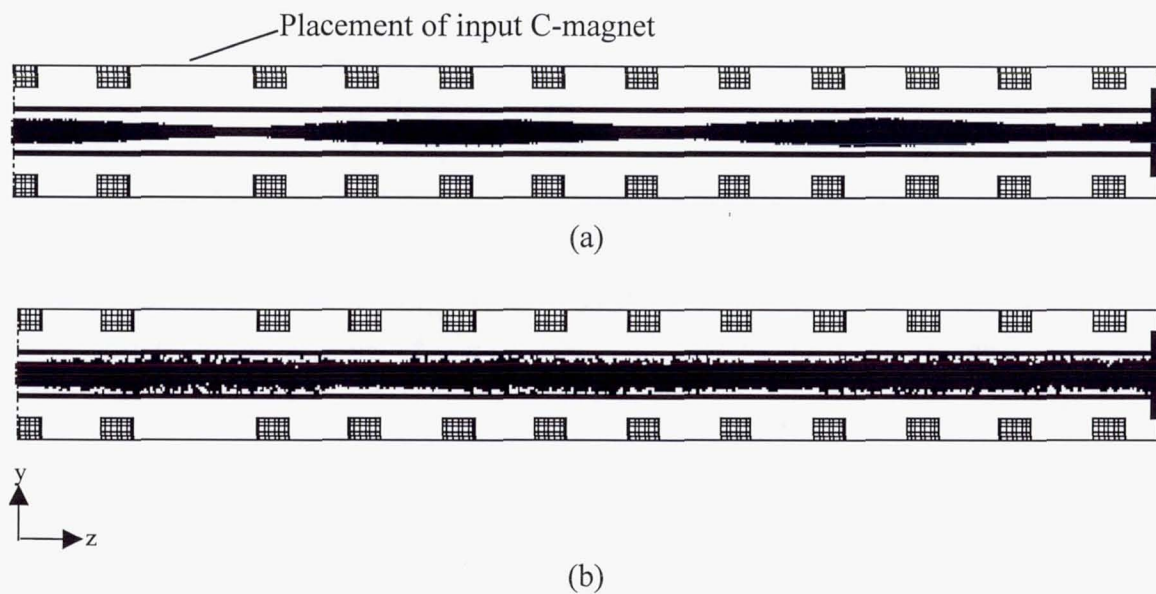


Figure 8 Two-dimensional beam profiles for several periods of PPM stack including input C-magnet (a) without initial transverse velocities and (b) with initial transverse velocities

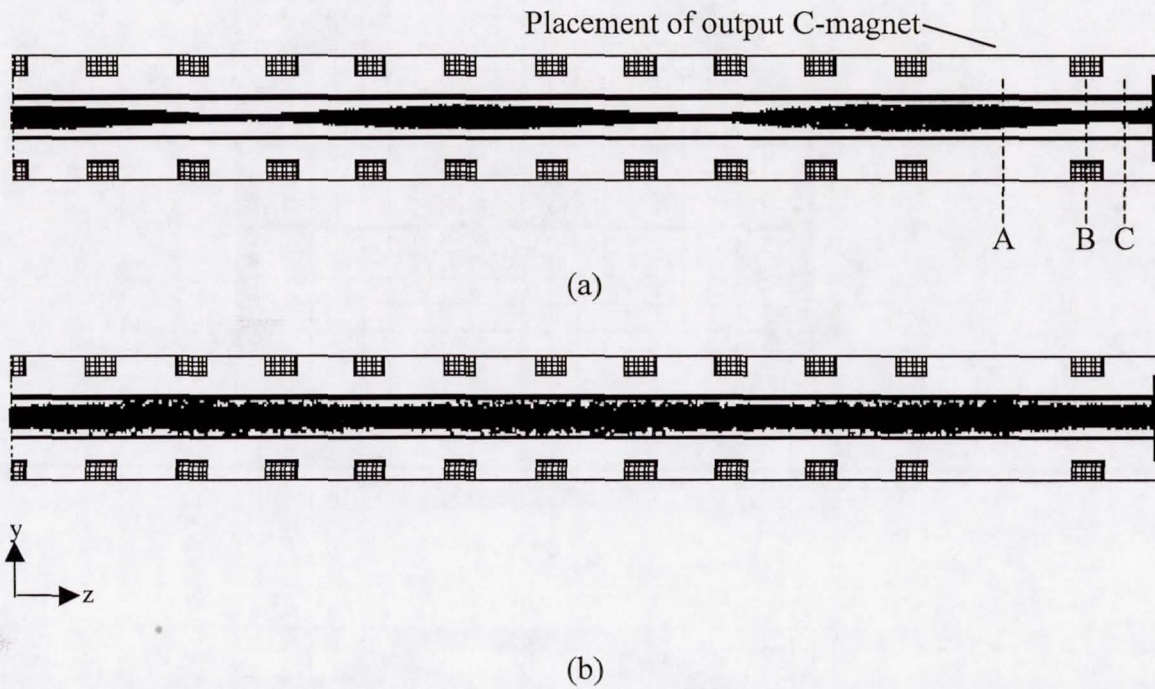
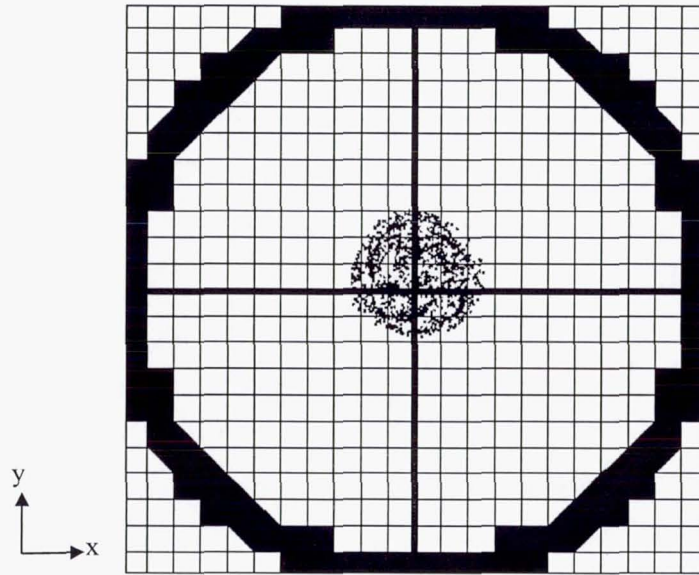
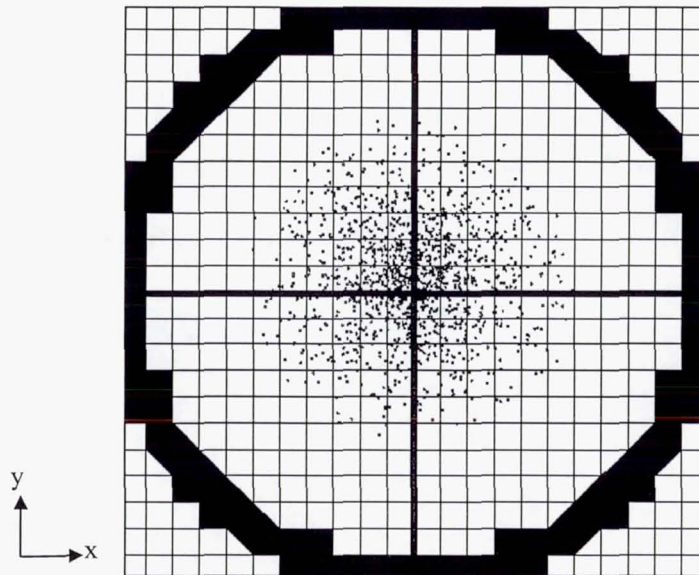


Figure 9 Two-dimensional beam profiles for several periods of PPM stack including output C-magnet (a) without initial transverse velocities and (b) with initial transverse velocities.



(a)



(b)

Figure 10 Cross-sectional view of the beam at point B of Figure 9 for PPM stack including output C-magnet (a) without initial transverse velocities and (b) with initial transverse velocities.

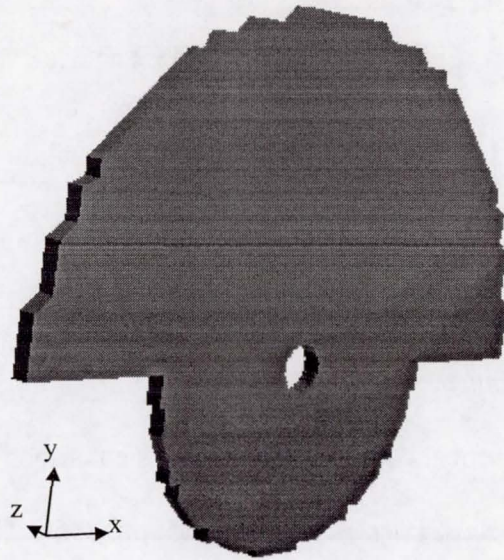


Figure 11 Simulated pole piece with shunt approximated by half-washer.

VII. REFERENCES

- i X. Zhai, J. T. Burdette, R. A. Brown and D. S. Komm, *Hughes Electron Dynamics*,
Circumferentially – Segmented Multistage Collector Experiment, *Work partially
supported by NASA Contract #NAS3-27363*.
- ii. T. Weiland, On the numerical solution of Maxwell's equations and applications in the
field of accelerator physics, *Part. Accel.*, Vol. 15, pp. 245-292, 1984.
- iii. T. Weiland, On the unique numerical solution of Maxwellian eigenvalue problems in
three dimensions, *Part. Accel.*, Vol. 17, pp. 227-242, 1985.
- iv Personal communication with Will Menninger of Hughes Electron Dynamics, August
1997.
- v Personal communication with Xiaoling Zhai of Hughes Electron Dynamics, June 1998.
- vi C. L. Kory, Three-dimensional simulations of PPM Focused Helical Traveling-wave
tubes, Dissertation for Doctor of Engineering, Cleveland State University, Cleveland,
Ohio, May 2000.
- vii The MAFIA Collaboration, *MAFIA TS3 the 3D-PIC Solver*, December 9 1996.
- viii A. S. Gilmour, Jr., *Principles of Traveling-Wave Tubes*, Norwood, MA: Artech
House, p.170, 1994.